NANO LETTERS

pubs.acs.org/NanoLett

Letter

Poly-β-cyclodextrin Supramolecular Nanoassembly with a pH-Sensitive Switch Removing Lysosomal Cholesterol Crystals for Antiatherosclerosis

Yan Zhang,[§] Fanglin Gong,[§] Yue Wu, Siyuan Hou, Lingjing Xue, Zhigui Su,* and Can Zhang*

Cite This: *Nano Lett.* 2021, 21, 9736−9745

Read Online

ABSTRACT: Cholesterol crystals (CCs), originally accumulating in the lysosome of cholesterol-laden cells, can aggravate the progression of atherosclerosis. β-cyclodextrin (CD) is a potent cholesterol acceptor or CC solubilizer. However, the random extraction of cholesterol impedes the *in vivo* application of CD for removing lysosomal CCs. Here, we exploit poly-β-cyclodextrin (pCD) as a lysosomal CC solubilizer and dextran sulfate grafted with benzimidazole (BM) as a pH-sensitive switch (pBM) to self-assemble into a supramolecular nanoassembly (pCD/pBM-SNA). The CD cavity in pCD/pBM-SNA can be efficiently sealed by hydrophobic BM at pH 7.4 (OFF). After it enters the lysosome, pCD/pBM-SNA disassembles, recovers the CD cavity to dissolve CCs into free cholesterol due to the protonation of BM (ON), and reduces CCs, finally enhancing the cholesterol efflux and promoting atherosclerosis regression. Our findings provide an "OFF−ON" tactic to remove lysosomal CCs for antiatherosclerosis as well as other diseases such as Niemann−Pick type C diseases with excessive cholesterol accumulation in the lysosome.

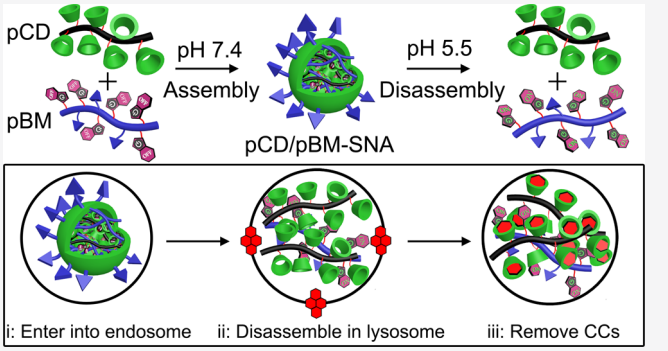

KEYWORDS: *atherosclerosis, cholesterol crystals, supramolecular nanoassembly, β-cyclodextrin, pH sensitive*

Atherosclerosis, one of the major causes of cardiovascular disease, is characterized by the deposition of a significant fibro-lipid burden and infiltration of immune cells under the artery wall.[1−4] Among the fibro-lipid burdens, cholesterol crystals (CCs) play an essential role in the progression of atherosclerosis.[5,6] It has been shown that CCs first generate and accumulate in the lysosome of cholesterol-laden cells after cholesterol enrichment by oxidized low-density lipoprotein (ox-LDL) and then gradually deposit in the atherosclerotic lesion as the apoptosis of cholesterol-laden cells.[7−9] The presence of CCs promotes chronic inflammation and the formation of necrotic cores by inducing the secretion of inflammatory cytokines such as IL-1β and TNF-α, enhancing the infiltration of monocytes and encouraging foam cells apoptosis.[6,10,11] Previous clinical data has shown that CCs, especially acicular crystals, are directly related to the formation of vulnerable atherosclerotic plaque, which are more likely to pierce the fibrous cap covering the surface of the plaque, resulting in plaque rupture, thrombosis formation, and the occurrence of cardiovascular and cerebrovascular diseases.[12,13]

It has been reported that only free cholesterol can be transported by cholesterol transporters in the lysosome such as Niemann−Pick type C related protein 1 or 2 (NPC-1 or NPC-2) for further metabolism and efflux intracellularly; once the free cholesterol is converted into CCs, they cannot be transported by NPC-1 or NPC-2, leading to the accumulation of massive CCs in the lysosome and cell apoptosis.[14,15] Therefore, the prevention of CC formation or the dissolution of CCs to free cholesterol in the lysosome to enhance the disposal of cholesterol will be of great clinical significance for atherosclerotic therapy. As confirmed by a recent study, the development of atherosclerosis can be halted by the treatment of cAMP-enhancing agents (such as forskolin, which catalyzes the production of cAMP,[16,17] and rolipram, which prevents the degradation of cAMP[18]) to inhibit the formation of CCs and promote cholesterol efflux in endothelial cells.[19] However, for macrophages or foam cells, which are the major cholesterol-laden cells in atherosclerotic plaque, none of the clinical drugs have been used to remove lysosomal CCs in macrophages or foam cells for the treatment of atherosclerosis.

β-cyclodextrin (CD) is composed of seven (α-1,4-)-linked glucose units and has a hydrophobic inner cavity and a

Received: September 21, 2021
Revised: November 1, 2021
Published: November 8, 2021

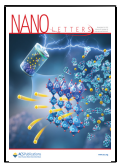

https://doi.org/10.1021/acs.nanolett.1c03664
Nano Lett. 2021, 21, 9736−9745

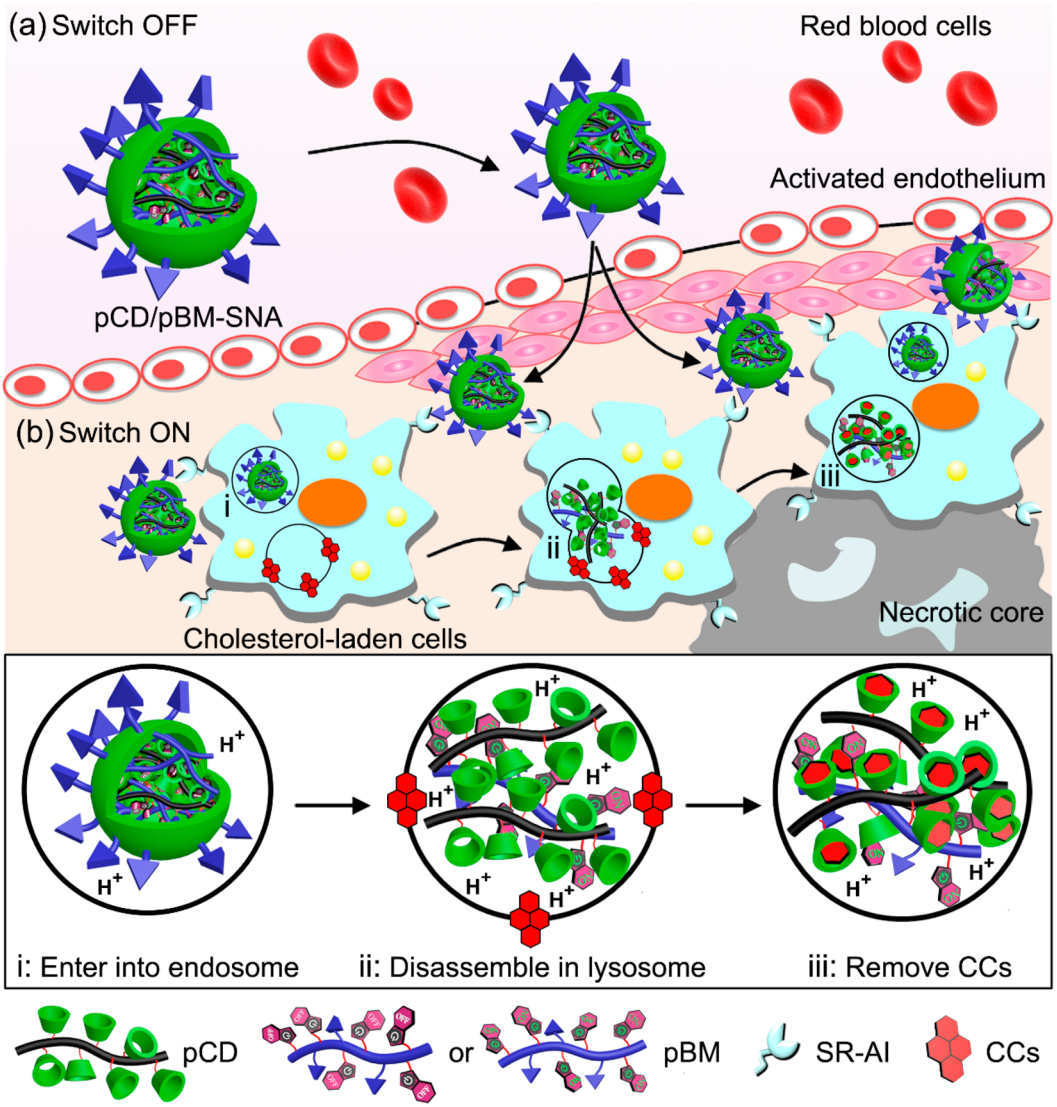

Figure 1. Schematic diagram of the poly-β-cyclodextrin supramolecular nanoassembly as a pH-sensitive lysosomal cholesterol crystal remover for antiatherosclerosis. (a) Switch OFF state of pCD/pBM-SNA. pCD/pBM-SNA turns off the CD cavity by sealing it with BM to prevent hemolysis and enters into the atherosclerotic plaque by enhanced permeability and retention (EPR) effects of the inflammatory endothelium. (b) Switch ON state of pCD/pBM-SNA: (i) pCD/pBM-SNA actively targets the cholesterol-laden cells by interaction between DS and SR-A1 and enters into endosome; (ii) pCD/pBM-SNA is transported into the lysosome intracellularly, disassembles, and recovers the CD cavity in the acidic lysosome; (iii) pCD mediates the solubilization and removal of CCs.

hydrophilic outer surface.[20] It has been reported that CD is a highly efficient cholesterol acceptor or solubilizer by an inclusion interaction because the size of the CD cavity matches well with the size of the cholesterol molecule.[21] Recently, the CD derivative of 2-hydroxypropyl-β-cyclodextrin (HP-β-CD) has been shown to have an antiatherosclerotic effect by reducing the CC load and augmenting reverse cholesterol transport of macrophages in the plaque after a high dose (2 g/kg) of subcutaneous injection in atherosclerosis animal models.[22] However, the direct exposure of the hydrophobic inner cavity of CD in the circulatory system will be confronted with many challenges. The CD cavity can extract cholesterol from cell membranes or lipoproteins that are circulating in the blood, which can lead to the premature occupation of the CD cavity before the dissolution of the CCs.[23] This would not only cause serious hemolysis in the blood and hearing loss[24−27] but also reduce the capacity for dissolving CCs. Second, the nonspecific biodistribution of CD as well as HP-β-CD *in vivo* further limits its use. In addition, it has been reported that the hydrophilic outer surface of CD hinders its capacity for membrane penetration and internalization by cells.[26] Recent studies showed that the CD cavity of methyl-β-cyclodextrin (M-β-CD) sealed with a hydrophobic statin could switch on again when it reaches a cholesterol-rich microenvironment, which would enhance the antiatherosclerosis effect of methyl-β-cyclodextrin.[28] However, whether this strategy could be used to remove CCs in the lysosome remains unclear. Therefore, a novel strategy that can safely and efficiently deliver CD to cholesterol-laden cells such as macrophages and foam cells to remove lysosomal CCs is required to hamper the progression of atherosclerosis.

Previous researches have shown that poly-β-cyclodextrin (pCD), as an important constituent in supramolecular chemistry, exhibits a higher binding intensity with hydrophobic molecules compared with that of CD due to multivalent inclusion interactions.[29−36] In the current study, we report

https://doi.org/10.1021/acs.nanolett.1c03664
Nano Lett. 2021, 21, 9736−9745

poly(isobutylene-*alt*-maleic anhydride) grafted with CD-NH_2 (pCD) for lysosomal CC removal and dextran sulfate (DS) grafted with benzimidazole (pBM) as a pH-sensitive switch to engineer a supramolecular nanoassembly (pCD/pBM-SNA). Poly(isobutylene-*alt*-maleic anhydride) was chosen because the anhydride moiety could readily react with the primary amine groups of CD-NH_2 under mild conditions, resulting in a high grafting efficiency.[29] In addition, the enhanced hydrophilicity of pCD due to the carboxylate group in the polymer chain and the hydrophilic outer surface of CD would further increase the solubility of complexes of pCD and cholesterol, which would decrease the tendency of complexes of pCD and cholesterol to crystallize again. We chose DS as the polymer backbone of BM because DS could actively target the scavenger receptor A1 (SR-A1), which is overexpressed on the surface of cholesterol-laden cells (macrophages or foam cells) in atherosclerotic plaque, and could improve the uptake of the supramolecular nanoassembly by SR-A1-mediated endocytosis and the transportation into the lysosomes.[37−40] Moreover, BM (pK_a 5.67) was utilized as a pH-sensitive switch because of its pH-dependent protonation and change in association constant with the CD cavity.[41,42] Under physiological conditions (pH 7.4), BM exhibited a hydrophobic property and a high association constant with the CD cavity, which facilitated the self-assembly of pCD/pBM-SNA by multivalent inclusion interactions between pCD and pBM, accompanied by sealing the CD cavity and preventing the extraction of cholesterol from the cell membrane or lipoproteins (switch OFF). When pCD/pBM-SNA was efficiently accumulated in atherosclerotic plaque, entered into cholesterol-laden cells such as macrophages or foam cells by SR-A1 mediated endocytosis, and fused with the acidic lysosome (pH 4−6), the association constant between BM and the CD cavity decreased to a very low level due to the change in BM from hydrophobic to hydrophilic after protonation. This transition led to the disassociation of BM from the CD cavity, the disassembly of pCD/pBM-SNA (switch ON), and the recovery of the capacity of pCD to solubilize CCs for antiatherosclerosis (Figure 1).

pCD and pBM were first synthesized (Schemes S1 and S2) and characterized by ^{1}H NMR spectroscopy, elemental analysis, and FTIR spectroscopy (Figure S1). A ^{1}H NMR and elemental analysis revealed that the pCD and pBM contained 15 CDs and 5 BMs, respectively, in each polymer backbone. We hypothesized that pCD and pBM could self-assemble into pCD/pBM-SNA at pH 7.4 and switch off the CD cavity by sealing it with BM (Figure 2a). The formation of pCD/pBM-SNA was monitored by dynamic light scattering (DLS). The results showed a remarkable decrease in the particle size as the ratio between CD and BM was varied from 1:0 to 1:2; the equilibrium value of the particle size was approximately 80 nm (Figure 2b), which suggested that the self-assembly and size control of pCD/pBM-SNA mainly depended on the multivalent inclusion interactions between pCD and pBM. Furthermore, the repulsive electrostatic interactions between the negatively charged carboxylate group in pCD and the negatively charged sulfate group in pBM also played a crucial role in modulating the particle size.[43,44] The formation of particles in the pCD solution (1:0) might be due to the hydrogen-bonding interactions of pCD.[29] In addition, the hemolysis of pCD was effectively prevented when pCD self-assembled into a supramolecular nanoassembly, and only 2% hemolysis occurred even at a ratio of 1:0.1 between CD and BM, indicating that the CD cavity remained in the OFF state (Figure 2c). The results also implied that there could be other factors that prevent hemolysis, such as the steric effect between pCD/pBM-SNA and red blood cells.[23] To obtain a suitable particle size for enhanced permeability and retention (EPR) effects of the inflammatory endothelium in atherosclerotic plaque as well as to avoid hemolysis, an optimized CD/BM molar ratio of 1:1 was used to construct pCD/pBM-SNA for all of the following investigations. The final pCD/pBM-SNA had a particle size of approximately 80 nm and a ζ potential of approximately −16 mV with good dispersity (Figure S2a,b). Moreover, the pCD/pBM-SNA also showed remarkable colloidal stability in PBS (pH 7.4) and serum during incubation for 12 h (Figure S2c), which was essential for its biological performance *in vivo*.[45]

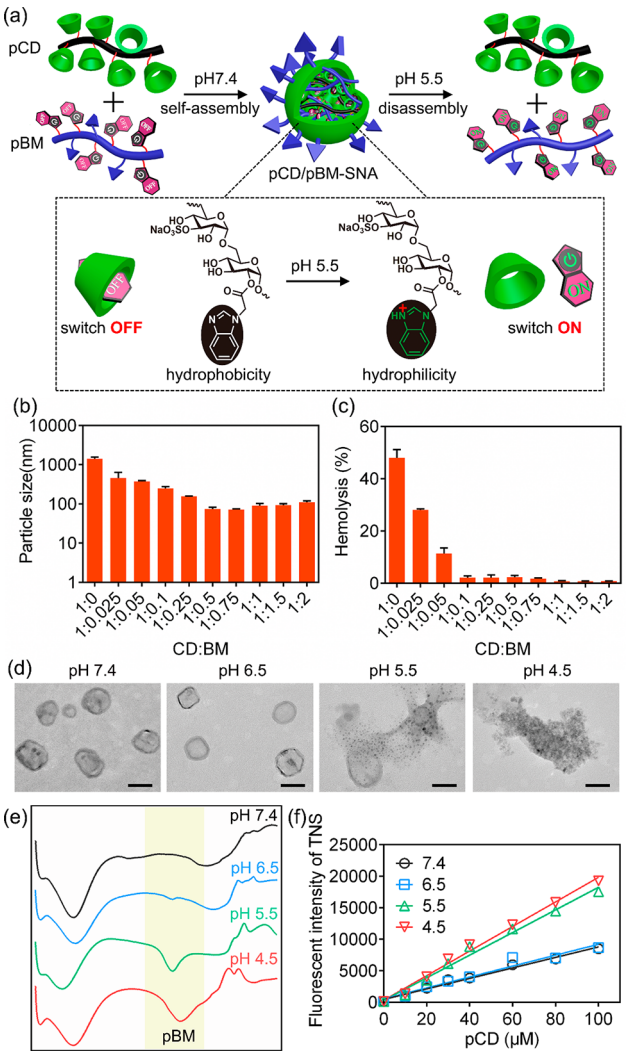

Figure 2. pH-sensitive self-assembly (switch OFF) and disassembly (switch ON) of pCD/pBM-SNA. (a) Schematic diagram of self-assembly (switch OFF the CD cavity) and disassembly (switch ON the CD cavity) of pCD/pBM-SNA at pH 7.4 and 5.5. (b) Influence of the CD/BM ratio on the particle size of pCD/pBM-SNA determined by DLS. Data points represent mean ± SD (n = 3). (c) Influence of the CD/BM ratio on the hemolysis of pCD/pBM-SNA under physiological conditions. Data points represent mean ± SD (n = 3). (d) TEM images of pCD/pBM-SNA at different pH values (pH 7.4, 6.5, 5.5, and 4.5). Scale bar: 50 nm. (e) Differential scanning calorimetry (DSC) spectra of pCD/pBM-SNA at different pH values (pH 7.4, 6.5, 5.5, and 4.5). (f) Change in fluorescence intensity of TNS incubated with pCD/pBM-SNA at different pH values (pH 7.4, 6.5, 5.5, and 4.5).

Because the CCs initially accumulate in the lysosome, in which the pH is approximately 4−6, we further investigated

https://doi.org/10.1021/acs.nanolett.1c03664
Nano Lett. 2021, 21, 9736−9745

whether pCD/pBM-SNA could show switchable "OFF−ON" in response to different pH values (pH 7.4, 6.5, 5.5, and 4.5). First, transmission electron microscopy (TEM) was used to observe the self-assembly (switch OFF) and disassembly (switch ON) of pCD/pBM-SNA at different pH values. The TEM images showed that the morphology of pCD/pBM-SNA remained intact at pH 7.4 and 6.5 and had a particle size of approximately 60 nm, whereas pCD/pBM-SNA began to disassemble at pH 5.5 and no pCD/pBM-SNA was observed at pH 4.5 (Figure 2d). Furthermore, the reduced count ratio of pCD/pBM-SNA, determined by DLS, confirmed that the amount of pCD/pBM-SNA was reduced with the disassembly of pCD/pBM-SNA when the pH decreased (Figure S3). The thermal property of pCD/pBM-SNA at different pH values was investigated by DSC. The endothermic peak belonging to pBM was significantly enhanced as the pH decreased (Figure 2e), indicating that more pBM was released due to the disassembly of pCD/pBM-SNA. It has been reported that 6-(*p*-toluidino-2-naphthalenesulfonic acid) (TNS) could bind strongly to the CD cavity and enhance the fluorescence intensity of TNS. To illustrate that the disassembly of pCD/pBM-SNA could recover the CD cavity, TNS was incubated with pCD/pBM-SNA at different pH values. As shown in Figure 2f, the enhanced fluorescence intensity of TNS at pH 5.5 and 4.5 was more apparent than that at pH 7.4 and 6.5, suggesting that more CD cavities were exposed to bind to TNS when the pH decreased. These data revealed that the self-assembly and disassembly of pCD/pBM-SNA were pH-dependent, mainly resulting from the pH-dependent protonation of BM and the change in the association constant between the CD cavity and BM. This transition would liberate the CD cavity and recover the capacity of pCD to further solubilize CCs.

Next, we investigated the improvement of the interaction between pCD and CCs after the disassembly of pCD/pBM-SNA under the acidic conditions of lysosomes. To verify this hypothesis, an aminofluorescein (AF)-modified pCD (AF-pCD) was synthesized (Scheme S3), characterized (Figure S4), and used to construct a supramolecular nanoassembly (AF-pCD/pBM-SNA). Then, AF-pCD/pBM-SNA was incubated with CCs at different pH values and imaged by confocal laser scanning microscopy (CLSM). The results showed that the fluorescence signal on the surface of the CCs was significantly elevated when the pH decreased to 5.5 (Figure 3a), highlighting an effective switch ON of the CD cavity at a lower pH, leading to an improved adsorption of AF-pCD/pBM-SNA on the surface of the CCs. A flow cytometry analysis also confirmed the above results (Figure 3b). As shown in Figure 3c, the hemolysis of pCD/pBM-SNA was effectively restrained at pH 7.4 and 6.5 but reoccurred as the pH decreased. A similar hemolysis of pCD/pBM-SNA was found at pH 5.5 and 4.5, which was equal to that of free pCD. Furthermore, the capacity of pCD/pBM-SNA to solubilize CCs was significantly weaker than that of pCD at pH 7.4 and 6.5 because the CD cavity was occupied by BM in the OFF state. However, both pCD and pCD/pBM-SNA showed identical capacities for solubilizing CCs when the pH was decreased to 5.5 and 4.5 (Figure 3d). We found that pCD can accommodate the hydrophobic cholesterol molecules and form a nanostructure with a particle size of about 100−200 nm (Figure S5), and similar results were also found in the complexes of pCD and paclitaxel.[29] The above results indicate that the activated CD cavity under the acidic conditions of lysosomes could fully recover the functions of extracting cholesterol and dissolving CCs.

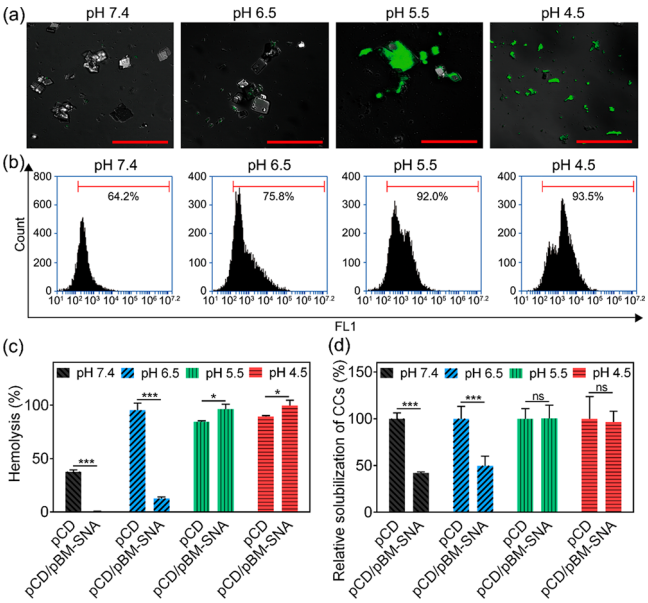

Figure 3. pH-sensitive improvement of the interaction between pCD/pBM-SNA and CCs. (a) Interaction between AF-pCD/pBM-SNA and CCs at different pH values (pH 7.4, 6.5, 5.5, and 4.5) observed by CLSM. Scale bar: 50 μm. (b) Interaction between AF-pCD/pBM-SNA and CCs at different pH values (pH 7.4, 6.5, 5.5, and 4.5) analyzed by flow cytometry. (c) Hemolysis of pCD and pCD/pBM-SNA at different pH values (pH 7.4, 6.5, 5.5, and 4.5). (d) Relative capacity of CC solubilization of pCD and pCD/pBM-SNA at different pH values (pH 7.4, 6.5, 5.5, and 4.5). Data points represent mean ± SD (n = 3). *P < 0.05, ***P < 0.001.

To test whether the pCD/pBM-SNA can remove the lysosomal CCs from cholesterol-laden cells *in vitro*, we selected bone marrow derived macrophage (BMDM) as a model cell to stimulate the generation of CCs through incubation with ox-LDL.[6] The generation of CCs in BMDM (CCs-BMDM) was confirmed by CLSM (Figure S6). The cytotoxicity of pCD/pBM-SNA against CCs-BMDM was detected by the MTT assay. No significant cytotoxicity toward CCs-BMDM was found after 24 h of incubation with pCD/pBM-SNA when the concentration of CD was lower than 2 mM (Figure S7). For 48 h incubation, the cytotoxicity of pCD/pBM-SNA against CCs-BMDM was concentration-dependent. Also, the ratio of cell viability was more than 75% when the concentration of CD was lower than 2 mM (Figure S7). In addition, AF-pCD/pBM-SNA was used to evaluate the cellular uptake by CCs-BMDM with a fluorescence microreader. The results showed that AF-pCD/pBM-SNA was effectively internalized and exhibited time-, concentration-, and energy-dependent properties (Figure S8a,b,e). The endocytosis process of the AF-pCD/pBM-SNA was significantly blocked by chlorpromazine (clathrin-mediated endocytosis) and nystatin (caveolin-mediated endocytosis), implying that the intracellular transport of AF-pCD/pBM-SNA may occur by endosome/lysosome pathways (Figure S8c).[46] Furthermore, a competitive inhibition study with excess DS further verified that the cellular uptake of AF-pCD/pBM-SNA relied on the interactions between DS and SR-A1 overexpressed on the surface of CCs-BMDM (Figure S8d). A previous report showed that SR-A1-mediated endocytosis also occurred by the endosome/lysosome pathway.[47] The intracellular transport of AF-pCD/pBM-SNA was also assessed by CLSM. As the incubation time was increased from 2 to 4 h, AF-pCD/pBM-SNA (green) colocalized with Lyso-Tracker labeling endo-

https://doi.org/10.1021/acs.nanolett.1c03664
Nano Lett. 2021, 21, 9736−9745

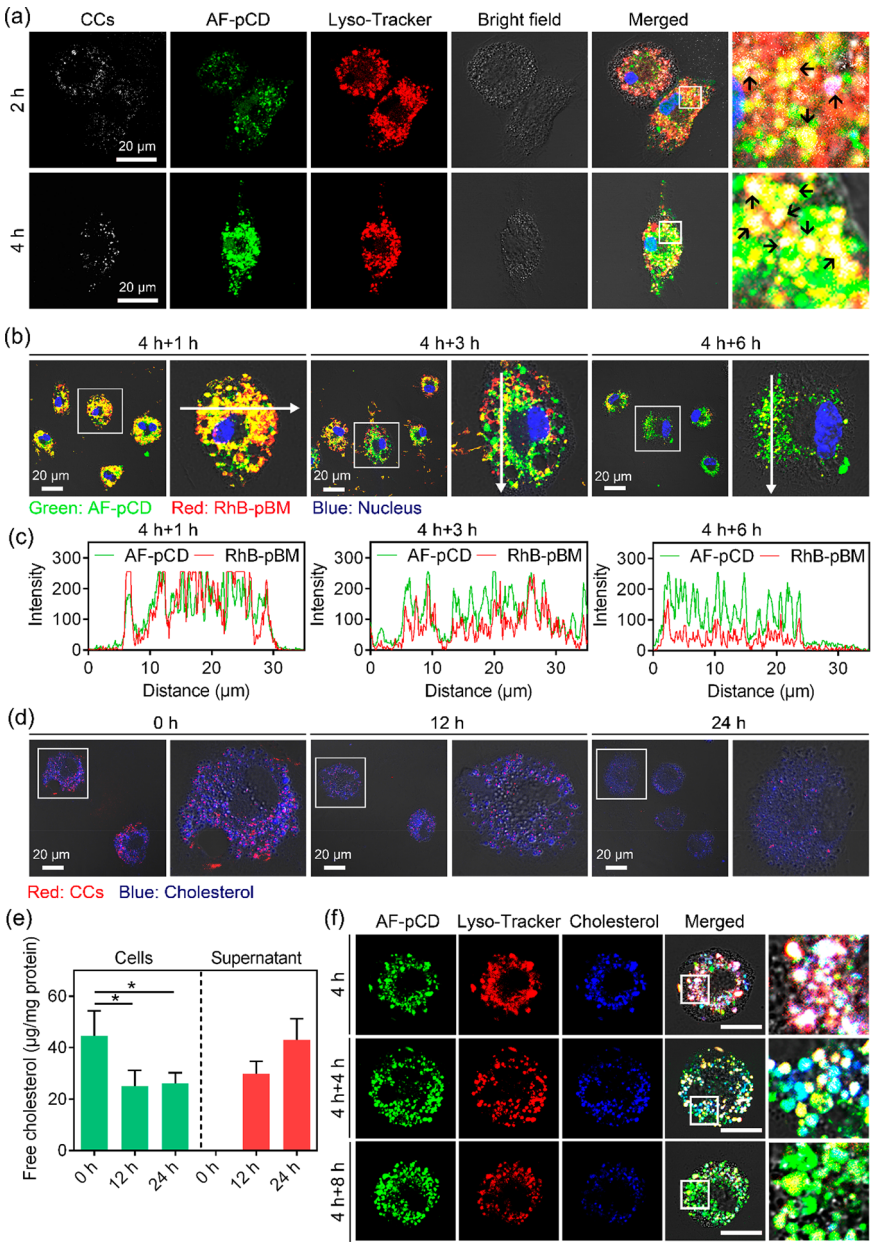

Figure 4. Colocalization, intracellular disassembly, removal of lysosomal CCs, and enhanced cholesterol efflux of pCD/pBM-SNA. (a) CLSM images of CCs-BMDM incubated with AF-pCD/pBM-SNA for 2 and 4 h. The black arrows indicate the colocalization of the AF-pCD/pBM-SNA with endosomes/lysosomes and CCs. (b) Intracellular disassembly of AF-pCD/RhB-pBM-SNA in CCs-BMDM after different incubation times. (c) Representative fluorescence signals of AF-pCD and RhB-pBM in CCs-BMDM after different incubation times. (d) *In vitro* removal of lysosomal CCs after treating CCs-BMDM with pCD/pBM-SNA for 0, 12, and 24 h. (e) Efflux of cholesterol from CCs-BMDM after the treatment of pCD/pBM-SNA for 0, 12, and 24 h. Data points represent mean ± SD ($n = 3$). $^*P < 0.05$. (f) Capacity of pCD/pBM-SNA to remove cholesterol in the lysosome. Scale bar: 20 μm.

some/lysosome (red) as well as the reflection fluorescence of CCs (white) in CCs-BMDM, evaluated by the increased yellow pixels and white pixels (Figure 4a). These results demonstrated that pCD/pBM-SNA could be effectively internalized and transported into endosome/lysosome intracellularly, finally colocalizing with lysosomal CCs.

To investigate the disassembly of pCD/pBM-SNA in CCs-BMDM, AF-pCD and Rhodamine B (RhB) -modified pBM (RhB-pBM) (Scheme S4 and Figure S4) were used to prepare a supramolecular nanoassembly (AF-pCD/RhB-pBM-SNA). The TEM images revealed that AF-pCD/RhB-pBM-SNA possessed a pH-sensitive assembly and disassembly (Figure S9). After incubation with CCs-BMDM for 4 h, AF-pCD/RhB-pBM-SNA was withdrawn and CCs-BMDM was incubated for another 1, 3, and 6 h in fresh culture medium. As shown in Figure 4b,c, after 1 h incubation most of the AF-pCD (green) and RhB-pBM (red) colocalized and yielded yellow fluorescence. Meanwhile, the fluorescence spectrum also revealed that the green and red signals were highly identical. The colocalization of AF-pCD and RhB-pBM became weak after 3 h of incubation along with a gradual separation of green and red signals. After 6 h of incubation, most of the green and red pixels separated, suggesting that AF-pCD and RhB-pBM dissociated and AF-pCD/RhB-pBM-SNA disassembled.

https://doi.org/10.1021/acs.nanolett.1c03664
Nano Lett. 2021, 21, 9736−9745

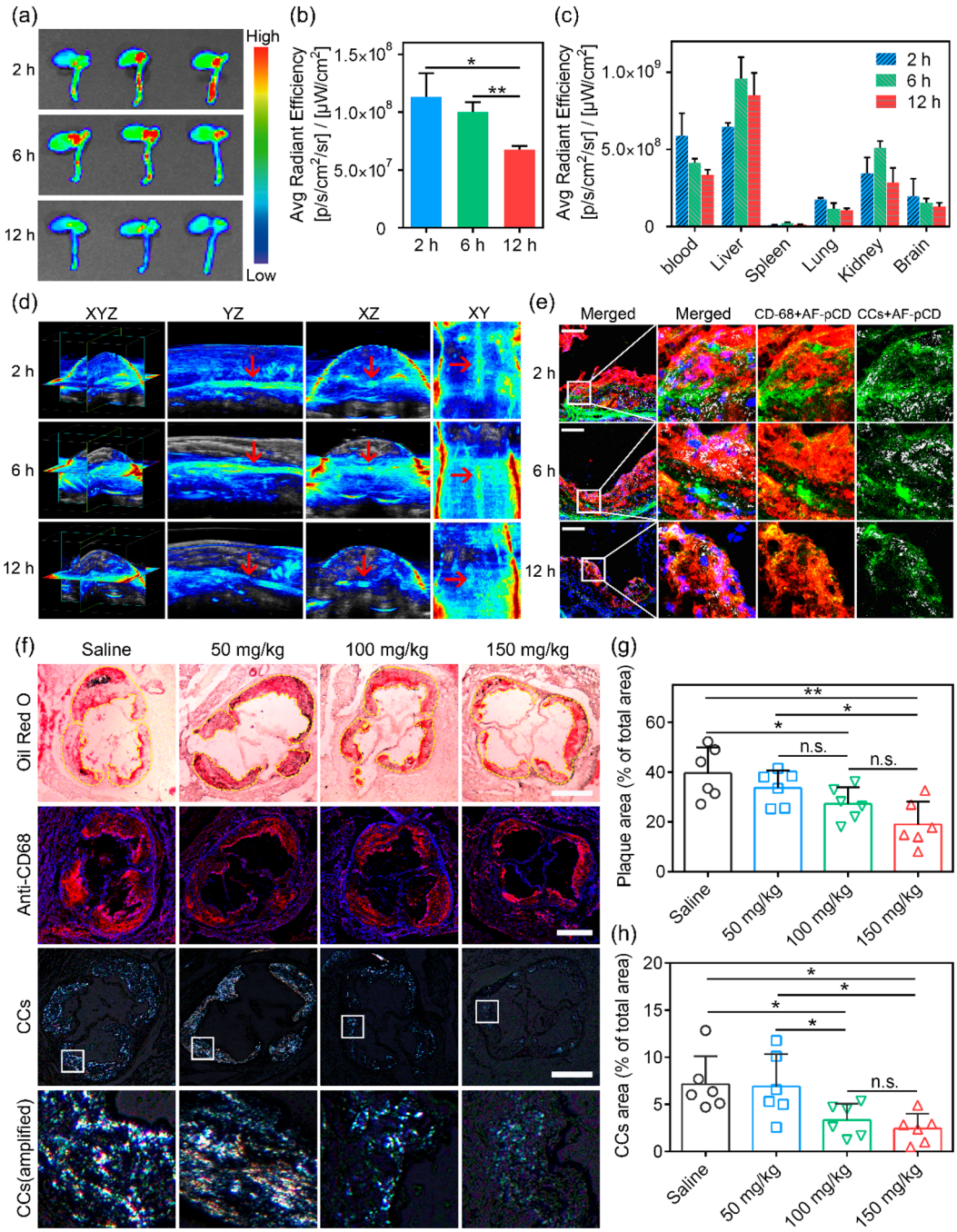

Figure 5. Atherosclerotic-plaque-targeting effect and therapeutic efficacy of pCD/pBM-SNA in ApoE$^{-/-}$ mice with atherosclerotic lesions. (a) Accumulation of AF-pCD/pBM-SNA in the heart/aorta using *ex vivo* imaging after 2, 6, and 12 h postinjection ($n = 3$). (b) Fluorescence intensity of the heart/aorta measured by an ROI assay after 2, 6, and 12 h postinjection of AF-pCD/pBM-SNA. Data points represent mean ± SD ($n = 3$). *$P < 0.05$, *$P < 0.01$. (c) Fluorescence intensity of blood and main organs measured by an ROI assay after 2, 6, and 12 h postinjection of AF-pCD/pBM-SNA. Data points represent mean ± SD ($n = 3$). (d) Time course of PA imaging of ApoE$^{-/-}$ mice after intravenous injection of Cy7-pCD/pBM-SNA. The red arrows indicate the aorta. (e) CLSM imaging of the freezing microtome section of the aortic root after administration of AF-pCD/pBM-SNA for 2, 6, and 12 h: (red) Alexa Fluor 647 Anti-CD68 antibody; (green) AF-pCD/pBM-SNA; (white) CCs; (blue) nucleus. Scale bar: 200 μm. (f) Aortic root sections were stained with Oil Red O to observe the development of atherosclerotic plaque, stained with Alexa Fluor 647 anti-CD68 to analyze the content of macrophages or foam cells, and visualized by polarized light microscopy to evaluate the formation of CCs. Scale bar: 400 μm. (g) The plaque area relative to the total aortic root area after treatment with pCD/pBM-SNA in ApoE$^{-/-}$ mice with atherosclerotic lesions. (h) The plaque CC area relative to the total aortic root area after treatment with pCD/pBM-SNA in ApoE$^{-/-}$ mice with atherosclerotic lesions. Data points represent mean ± SD ($n = 6$). *$P < 0.05$, **$P < 0.01$.

As shown in Figure 4a, large amounts of CCs were found in the lysosome. Furthermore, the *in vitro* effect of removing lysosomal CCs from CCs-BMDM by pCD/pBM-SNA was evaluated by CLSM. The results revealed that pCD/pBM-SNA markedly reduced the number of lysosomal CCs as well as cholesterol stained by filipin in CCs-BMDM after incubation for 12 and 24 h (Figure 4d) in comparison to 0 h. In addition, a quantitative analysis also showed that pCD/pBM-SNA

https://doi.org/10.1021/acs.nanolett.1c03664
Nano Lett. 2021, 21, 9736−9745

effectively improved the efflux of free cholesterol after incubation for 12 and 24 h, resulting in a decrease in the amount of free cholesterol intracellularly, while the amount of free cholesterol in the cellular supernatant was elevated (Figure 4e). Previous reports showed that β-CD derivatives could mobilize lysosomal-stored free cholesterol and decrease lysosomal cholesterol accumulation, bypassing the function of NPC-1 or NPC-2, finally enhancing cholesterol extracellular efflux.[48,49] To further elucidate the mechanism of enhanced lysosomal cholesterol efflux by pCD/pBM-SNA, CCs-BMDM was incubated with AF-pCD/pBM-SNA for various times. We found that AF-pCD/pBM-SNA colocalized with cholesterol in lysosomes after a 4 h incubation and then mobilized cholesterol out of lysosomes as the incubation time was increased to 8 h. After 12 h of incubation, cholesterol in lysosomes remarkably decreased (Figure 4f). It has been reported that the expression of a cholesterol-related ATP-binding cassette (ABC) transporter, such as ABCA1, played an important role in cholesterol efflux.[50] In this study, expression of ABCA1 in CCs-BMDM was reduced on incubation with pCD/pBM-SNA from 0 to 36 h (Figure S10). According to a previous study, the downregulation of expression of ABCA1 could be due to cholesterol lowering by pCD/pBM-SNA.[51] These results suggest that the enhanced efflux of cholesterol by pCD/pBM-SNA was independent of the function of ABCA1, which was similar to the function of HP-β-CD.[22]

To evaluate the atherosclerotic-plaque-targeting effect of pCD/pBM-SNA *in vivo*, ApoE$^{-/-}$ mice with atherosclerotic plaque were intravenously administered with AF-pCD/pBM-SNA. As shown in Figure 5a,b, after 2 and 6 h postinjection, AF-pCD/pBM-SNA efficiently accumulated at the aorta and aortic root where it was apt to form plaques, and the fluorescence signals decreased as the time was extended to 12 h. The biodistribution revealed that AF-pCD/pBM-SNA possessed a good, long circulating effect, and the accumulation of AF-pCD/pBM-SNA in the liver and kidney implied that AF-pCD/pBM-SNA would be metabolized in the liver and eliminated in the kidney (Figure 5c and Figure S11). Meanwhile, photoacoustic (PA) imaging was also applied to investigate the targeting capacity of Cy7-labeled pCD/pBM-SNA (Cy7-pCD/pBM-SNA) *in vivo*. The PA imaging showed an enhanced PA signal in the aorta (Figure 5d), which further confirmed that pCD/pBM-SNA could be delivered to the region with plaques. Similarly to the *ex vivo* study, the intensity of the PA signal decreased over time. In addition, the CLSM imaging of aortic root sections showed that AF-pCD/pBM-SNA colocalized with macrophages or foam cells (anti-CD68 labeled) and CCs (white) in the atherosclerotic plaque (Figure 5e). The targeting capacity of pCD/pBM-SNA to the atherosclerotic plaque may result from the EPR effects of the inflammatory endothelium and the active targeting effect of DS through the interaction with SR-A1 overexpression on the surface of the macrophages or foam cells in the atherosclerotic plaque, which would be beneficial to removing lysosomal CCs from plaques.

To evaluate the effect of pCD/pBM-SNA treatment on the reduction of CCs and the improvement of atherosclerotic regression *in vivo*, ApoE$^{-/-}$ mice with atherosclerotic lesions were treated for 2 weeks, during which the mice were continuously fed with the Western diet. The mice received 50, 100, and 150 mg/kg of pCD/pBM-SNA every other day; free pCD could not be used because it can induce severe hemolysis of human erythrocytes even at a low dose (50 mg/kg) of pCD/pBM-SNA. As shown in Figure 5f, the treatment with pCD/pBM-SNA could decrease the atherosclerotic plaque size, the CD68-marked macrophages or foam cells, and the CC load within the aortic root in a dosage-dependent manner. The treatment of pCD/pBM-SNA at a high dosage resulted in the strongest antiatherosclerotic capability (Figure 5g,h). The improvement in the therapeutic effect of pCD/pBM-SNA at a high dosage could be ascribed to the targeted delivery to atherosclerotic plaque and efficient solubilization of lysosomal CCs into free cholesterol. Free cholesterol dissolved by pCD would be further metabolized into water-soluble oxysterols for diffusion extracellularly or nontoxic cholesteryl esters for storage intracellularly, respectively.[22,52] Meanwhile, free cholesterol would be transferred to high-density lipoprotein for reverse cholesterol transport to the liver.[53] Moreover, cholesterol in a complex with pCD might enter into blood circulation, in which cholesterol would be released from the complex and exchange with lipoproteins for further disposal.[54] In addition, a safety evaluation of pCD/pBM-SNA showed that no significant differences were found in the hemogram and pathologic analysis from the H&E staining images of the heart, liver, spleen, lung, kidney, and brain in comparison with the saline group (Figures S12 and S13). In addition, the influence of pCD/pBM-SNA on the serum cholesterol homeostasis *in vivo* was investigated. As shown in Figure S14, no significant differences were found in the total cholesterol, free cholesterol and cholesterol ester in the serum after the intravenous administration of pCD/pBM-SNA in comparison with saline, suggesting that pCD/pBM-SNA has good biocompatibility.

In summary, we present a pH-sensitive controllable "OFF−ON" therapeutic strategy based on pCD/pBM-SNA for the removal of lysosomal CCs from cholesterol-laden cells in atherosclerotic plaque. In a physiological environment with pH 7.4, pCD/pBM-SNA restrains the interaction between the CD cavity and cholesterol by sealing with hydrophobic BM, prevents random extraction of cholesterol, and further improves its biosafety and tolerability (switch OFF). After it enters the lysosome, pCD/pBM-SNA exhibits a pH-sensitive disassembly and switches on the CD cavity again due to the protonation of BM (switch ON), which recovers the capacity of dissolution of CCs and enhances the cholesterol efflux, finally remarkably removing CCs from atherosclerotic plaque and improving the regression of atherosclerosis. These findings suggest that pCD/pBM-SNA would be a potential platform for removing lysosomal CCs, which not only resolves the progression of atherosclerosis but also deserves study in the future in other diseases such as Niemann−Pick type C diseases with the lysosomal accumulation of excessive cholesterol.

■ ASSOCIATED CONTENT

Supporting Information

The Supporting Information is available free of charge at https://pubs.acs.org/doi/10.1021/acs.nanolett.1c03664.

Details of experimental materials and methods, characteristics of pCD and pBM, physicochemical properties of pCD/pBM-SNA, count rate of pCD/pBM-SNA at different pH values, fluorescence spectra of AF-pCD and RhB-pBM, CC imaging in CCs-BMDM, cytotoxicity of pCD/pBM-SNA, endocytosis mechanism of pCD/pBM-SNA, TEM images of AF-pCD/RhB-pBM-SM, Western blot analysis of ABCA1, biodistribution of AF-pCD/pBM-SNA, hemogram analysis, HE staining

https://doi.org/10.1021/acs.nanolett.1c03664
Nano Lett. 2021, 21, 9736−9745

images, and the serum cholesterol homeostasis *in vivo* (PDF)

AUTHOR INFORMATION

Corresponding Authors

Zhigui Su − *State Key Laboratory of Natural Medicines, Center of Advanced Pharmaceuticals and Biomaterials, Jiangsu Key Laboratory of Drug Discovery for Metabolic Diseases and School of Pharmacy, China Pharmaceutical University, Nanjing 210009, People's Republic of China*; Email: zhiguisu707@cpu.edu.cn

Can Zhang − *State Key Laboratory of Natural Medicines, Center of Advanced Pharmaceuticals and Biomaterials, Jiangsu Key Laboratory of Drug Discovery for Metabolic Diseases, China Pharmaceutical University, Nanjing 210009, People's Republic of China*; orcid.org/0000-0003-3529-5438; Email: zhangcan@cpu.edu.cn

Authors

Yan Zhang − *State Key Laboratory of Natural Medicines, Center of Advanced Pharmaceuticals and Biomaterials, Jiangsu Key Laboratory of Drug Discovery for Metabolic Diseases, China Pharmaceutical University, Nanjing 210009, People's Republic of China*

Fanglin Gong − *State Key Laboratory of Natural Medicines, Center of Advanced Pharmaceuticals and Biomaterials, Jiangsu Key Laboratory of Drug Discovery for Metabolic Diseases and School of Pharmacy, China Pharmaceutical University, Nanjing 210009, People's Republic of China*

Yue Wu − *State Key Laboratory of Natural Medicines, Center of Advanced Pharmaceuticals and Biomaterials, Jiangsu Key Laboratory of Drug Discovery for Metabolic Diseases and School of Pharmacy, China Pharmaceutical University, Nanjing 210009, People's Republic of China*

Siyuan Hou − *State Key Laboratory of Natural Medicines, Center of Advanced Pharmaceuticals and Biomaterials, Jiangsu Key Laboratory of Drug Discovery for Metabolic Diseases, China Pharmaceutical University, Nanjing 210009, People's Republic of China*

Lingjing Xue − *State Key Laboratory of Natural Medicines, Center of Advanced Pharmaceuticals and Biomaterials, Jiangsu Key Laboratory of Drug Discovery for Metabolic Diseases, China Pharmaceutical University, Nanjing 210009, People's Republic of China*

Complete contact information is available at: https://pubs.acs.org/10.1021/acs.nanolett.1c03664

Author Contributions

[§]Y.Z. and F.G. contributed equally to this work.

Author Contributions

Y.Z., Z.S., and C.Z. designed the research. Y.Z., F.G., Z.S., Y.W., and L.X. performed the experiments. Y.Z., F.G., Z.S., and C.Z. analyzed the data. Y.Z., Z.S., S.H., and C.Z. wrote the manuscript. All of the authors read and approved the final manuscript.

Notes

The authors declare no competing financial interest.

ACKNOWLEDGMENTS

This work was supported by the National Natural Science Foundation of China (No. 81973270, 81930099, 82130102, 81773664), the Natural Science Foundation of Jiangsu Province (BK20212011), the Natural Science Foundation of Jiangsu Province of China for Excellent Young Scholars (No. BK20190078), "Double First-Class" University project (CPU2018GY47, CPU2018GF10), 111 Project from the Ministry of Education of China and the State Administration of Foreign Expert Affairs of China (No.111-2-07, B17047), and the Open Project of State Key Laboratory of Natural Medicines (No. SKLNMZZ202017). The authors thank the public platform of State Key Laboratory of Natural Medicines for assistance with confocal microscopy, flow cytometry and photoacoustic imaging.

REFERENCES

(1) GBD 2016 Causes of Death Collaborators. Global, regional, and national age-sex specific mortality for 264 causes of death, 1980−2016: a systematic analysis for the Global Burden of Disease Study 2016. *Lancet* **2017**, *390* (10100), 1151−1210.

(2) Maxfield, F. R.; Tabas, I. Role of cholesterol and lipid organization in disease. *Nature* **2005**, *438* (7068), 612−621.

(3) Hansson, G. K.; Hermansson, A. The immune system in atherosclerosis. *Nat. Immunol.* **2011**, *12* (3), 204−212.

(4) Libby, P.; Ridker, P. M.; Hansson, G. K. Progress and challenges in translating the biology of atherosclerosis. *Nature* **2011**, *473* (7347), 317−325.

(5) Janoudi, A.; Shamoun, F. E.; Kalavakunta, J. K.; Abela, G. S. Cholesterol crystal induced arterial inflammation and destabilization of atherosclerotic plaque. *Eur. Heart J.* **2016**, *37* (25), 1959−1967.

(6) Duewell, P.; Kono, H.; Rayner, K. J.; Sirois, C. M.; Vladimer, G.; Bauernfeind, F. G.; Abela, G. S.; Franchi, L.; Nunez, G.; Schnurr, M.; Espevik, T.; Lien, E.; Fitzgerald, K. A.; Rock, K. L.; Moore, K. J.; Wright, S. D.; Hornung, V.; Latz, E. NLRP3 inflammasomes are required for atherogenesis and activated by cholesterol crystals. *Nature* **2010**, *464* (7293), 1357−1361.

(7) Tangirala, R. K.; Jerome, W. G.; Jones, N. L.; Small, D. M.; Johnson, W. J.; Glick, J. M.; Mahlberg, F. H.; Rothblat, G. H. Formation of cholesterol monohydrate crystals in macrophage-derived foam cells. *J. Lipid Res.* **1994**, *35* (1), 93−104.

(8) Kellner-Weibel, G.; Yancey, P. G.; Jerome, W. G.; Walser, T.; Mason, R. P.; Phillips, M. C.; Rothblat, G. H. Crystallization of free cholesterol in model macrophage foam cells. *Arterioscler., Thromb., Vasc. Biol.* **1999**, *19* (8), 1891−1898.

(9) Varsano, N.; Dadosh, T.; Kapishnikov, S.; Pereiro, E.; Shimoni, E.; Jin, X.; Kruth, H. S.; Leiserowitz, L.; Addadi, L. Development of Correlative Cryo-soft X-ray Tomography and Stochastic Reconstruction Microscopy. A Study of Cholesterol Crystal Early Formation in Cells. *J. Am. Chem. Soc.* **2016**, *138* (45), 14931−14940.

(10) Warnatsch, A.; Ioannou, M.; Wang, Q.; Papayannopoulos, V. Inflammation. Neutrophil extracellular traps license macrophages for cytokine production in atherosclerosis. *Science* **2015**, *349* (6245), 316−320.

(11) Corr, E. M.; Cunningham, C. C.; Dunne, A. Cholesterol crystals activate Syk and PI3 kinase in human macrophages and dendritic cells. *Atherosclerosis* **2016**, *251*, 197−205.

(12) Abela, G. S.; Aziz, K.; Vedre, A.; Pathak, D. R.; Talbott, J. D.; Dejong, J. Effect of cholesterol crystals on plaques and intima in arteries of patients with acute coronary and cerebrovascular syndromes. *Am. J. Cardiol.* **2009**, *103* (7), 959−968.

(13) Kataoka, Y.; Puri, R.; Hammadah, M.; Duggal, B.; Uno, K.; Kapadia, S. R.; Tuzcu, E. M.; Nissen, S. E.; Nicholls, S. J. Cholesterol crystals associate with coronary plaque vulnerability in vivo. *J. Am. Coll. Cardiol.* **2015**, *65* (6), 630−632.

(14) Sleat, D. E.; Wiseman, J. A.; El-Banna, M.; Price, S. M.; Verot, L.; Shen, M. M.; Tint, G. S.; Vanier, M. T.; Walkley, S. U.; Lobel, P. Genetic evidence for nonredundant functional cooperativity between NPC1 and NPC2 in lipid transport. *Proc. Natl. Acad. Sci. U. S. A.* **2004**, *101* (16), 5886−5891.

(15) Chu, B. B.; Liao, Y. C.; Qi, W.; Xie, C.; Du, X.; Wang, J.; Yang, H.; Miao, H. H.; Li, B. L.; Song, B. L. Cholesterol transport through

lysosome-peroxisome membrane contacts. *Cell* **2015**, *161* (2), 291−306.
(16) Kilmer, S. L.; Carlsen, R. C. Forskolin activation of adenylate cyclase in vivo stimulates nerve regeneration. *Nature* **1984**, *307* (5950), 455−457.
(17) Hao, H.; Ma, X.; Chen, H.; Zhu, L.; Xu, Z.; Li, Q.; Xu, C.; Zhang, Y.; Peng, Z.; Wang, M. The cyclic adenosine monophosphate elevating medicine, forskolin, reduces neointimal formation and atherogenesis in mice. *J. Cell. Mol. Med.* **2020**, *24* (17), 9638−9645.
(18) Sommer, N.; Loschmann, P. A.; Northoff, G. H.; Weller, M.; Steinbrecher, A.; Steinbach, J. P.; Lichtenfels, R.; Meyermann, R.; Riethmuller, A.; Fontana, A.; et al. The antidepressant rolipram suppresses cytokine production and prevents autoimmune encephalomyelitis. *Nat. Med.* **1995**, *1* (3), 244−248.
(19) Baumer, Y.; McCurdy, S.; Weatherby, T. M.; Mehta, N. N.; Halbherr, S.; Halbherr, P.; Yamazaki, N.; Boisvert, W. A. Hyperlipidemia-induced cholesterol crystal production by endothelial cells promotes atherogenesis. *Nat. Commun.* **2017**, *8* (1), 1129.
(20) Crini, G. Review: a history of cyclodextrins. *Chem. Rev.* **2014**, *114* (21), 10940−10975.
(21) Yu, Y.; Chipot, C.; Cai, W.; Shao, X. Molecular dynamics study of the inclusion of cholesterol into cyclodextrins. *J. Phys. Chem. B* **2006**, *110* (12), 6372−6378.
(22) Zimmer, S.; Grebe, A.; Bakke, S. S.; Bode, N.; Halvorsen, B.; Ulas, T.; Skjelland, M.; De Nardo, D.; Labzin, L. I.; Kerksiek, A.; Hempel, C.; Heneka, M. T.; Hawxhurst, V.; Fitzgerald, M. L.; Trebicka, J.; Bjorkhem, I.; Gustafsson, J. A.; Westerterp, M.; Tall, A. R.; Wright, S. D.; Espevik, T.; Schultze, J. L.; Nickenig, G.; Lutjohann, D.; Latz, E. Cyclodextrin promotes atherosclerosis regression via macrophage reprogramming. *Sci. Transl. Med.* **2016**, *8* (333), 333ra50.
(23) Lopez, C. A.; de Vries, A. H.; Marrink, S. J. Computational microscopy of cyclodextrin mediated cholesterol extraction from lipid model membranes. *Sci. Rep.* **2013**, *3*, 2071.
(24) Irie, T.; Uekama, K. Pharmaceutical applications of cyclodextrins. III. Toxicological issues and safety evaluation. *J. Pharm. Sci.* **1997**, *86* (2), 147−162.
(25) Gould, S.; Scott, R. C. 2-Hydroxypropyl-beta-cyclodextrin (HP-beta-CD): a toxicology review. *Food Chem. Toxicol.* **2005**, *43* (10), 1451−1459.
(26) Brewster, M. E.; Loftsson, T. Cyclodextrins as pharmaceutical solubilizers. *Adv. Drug Delivery Rev.* **2007**, *59* (7), 645−666.
(27) Crumling, M. A.; King, K. A.; Duncan, R. K. Cyclodextrins and Iatrogenic Hearing Loss: New Drugs with Significant Risk. *Front. Cell. Neurosci.* **2017**, *11*, 355.
(28) Kim, H.; Kumar, S.; Kang, D. W.; Jo, H.; Park, J. H. Affinity-Driven Design of Cargo-Switching Nanoparticles to Leverage a Cholesterol-Rich Microenvironment for Atherosclerosis Therapy. *ACS Nano* **2020**, *14* (6), 6519−6531.
(29) Namgung, R.; Mi Lee, Y.; Kim, J.; Jang, Y.; Lee, B. H.; Kim, I. S.; Sokkar, P.; Rhee, Y. M.; Hoffman, A. S.; Kim, W. J. Poly-cyclodextrin and poly-paclitaxel nano-assembly for anticancer therapy. *Nat. Commun.* **2014**, *5*, 3702.
(30) Hu, Q. D.; Tang, G. P.; Chu, P. K. Cyclodextrin-based host-guest supramolecular nanoparticles for delivery: from design to applications. *Acc. Chem. Res.* **2014**, *47* (7), 2017−2025.
(31) Miyamae, K.; Nakahata, M.; Takashima, Y.; Harada, A. Self-Healing, Expansion-Contraction, and Shape-Memory Properties of a Preorganized Supramolecular Hydrogel through Host-Guest Interactions. *Angew. Chem., Int. Ed.* **2015**, *54* (31), 8984−8987.
(32) Schmidt, B.; Barner-Kowollik, C. Dynamic Macromolecular Material Design-The Versatility of Cyclodextrin-Based Host-Guest Chemistry. *Angew. Chem., Int. Ed.* **2017**, *56* (29), 8350−8369.
(33) Xiao, L. L.; Ling, Y. H.; Alsbaiee, A.; Li, C. J.; Helbling, D. E.; Dichtel, W. R. *β*-Cyclodextrin Polymer Network Sequesters Perfluorooctanoic Acid at Environmentally Relevant Concentrations. *J. Am. Chem. Soc.* **2017**, *139* (23), 7689−7692.
(34) Wang, L.; Li, L. L.; Fan, Y. S.; Wang, H. Host-guest supramolecular nanosystems for cancer diagnostics and therapeutics. *Adv. Mater.* **2013**, *25* (28), 3888−3898.
(35) Dong, R.; Zhou, Y.; Huang, X.; Zhu, X.; Lu, Y.; Shen, J. Functional supramolecular polymers for biomedical applications. *Adv. Mater.* **2015**, *27* (3), 498−526.
(36) Liu, G. T.; Yuan, Q. J.; Hollett, G.; Zhao, W.; Kang, Y.; Wu, J. Cyclodextrin-based host-guest supramolecular hydrogel and its application in biomedical fields. *Polym. Chem.* **2018**, *9* (25), 3436−3449.
(37) Suzuki, H.; Kurihara, Y.; Takeya, M.; Kamada, N.; Kataoka, M.; Jishage, K.; Ueda, O.; Sakaguchi, H.; Higashi, T.; Suzuki, T.; Takashima, Y.; Kawabe, Y.; Cynshi, O.; Wada, Y.; Honda, M.; Kurihara, H.; Aburatani, H.; Doi, T.; Matsumoto, A.; Azuma, S.; Noda, T.; Toyoda, Y.; Itakura, H.; Yazaki, Y.; Kodama, T.; et al. A role for macrophage scavenger receptors in atherosclerosis and susceptibility to infection. *Nature* **1997**, *386* (6622), 292−296.
(38) de Winther, M. P.; van Dijk, K. W.; Havekes, L. M.; Hofker, M. H. Macrophage scavenger receptor class A: A multifunctional receptor in atherosclerosis. *Arterioscler., Thromb., Vasc. Biol.* **2000**, *20* (2), 290−7.
(39) Kzhyshkowska, J.; Neyen, C.; Gordon, S. Role of macrophage scavenger receptors in atherosclerosis. *Immunobiology* **2012**, *217* (5), 492−502.
(40) Chao, Y.; Makale, M.; Karmali, P. P.; Sharikov, Y.; Tsigelny, I.; Merkulov, S.; Kesari, S.; Wrasidlo, W.; Ruoslahti, E.; Simberg, D. Recognition of dextran-superparamagnetic iron oxide nanoparticle conjugates (Feridex) via macrophage scavenger receptor charged domains. *Bioconjugate Chem.* **2012**, *23* (5), 1003−1009.
(41) Meng, H.; Xue, M.; Xia, T.; Zhao, Y. L.; Tamanoi, F.; Stoddart, J. F.; Zink, J. I.; Nel, A. E. Autonomous in vitro anticancer drug release from mesoporous silica nanoparticles by pH-sensitive nanovalves. *J. Am. Chem. Soc.* **2010**, *132* (36), 12690−12697.
(42) Xue, M.; Zhong, X.; Shaposhnik, Z.; Qu, Y.; Tamanoi, F.; Duan, X.; Zink, J. I. pH-Operated mechanized porous silicon nanoparticles. *J. Am. Chem. Soc.* **2011**, *133* (23), 8798−8801.
(43) Wang, H.; Wang, S.; Su, H.; Chen, K. J.; Armijo, A. L.; Lin, W. Y.; Wang, Y.; Sun, J.; Kamei, K.; Czernin, J.; Radu, C. G.; Tseng, H. R. A supramolecular approach for preparation of size-controlled nanoparticles. *Angew. Chem., Int. Ed.* **2009**, *48* (24), 4344−4348.
(44) Grana-Suarez, L.; Verboom, W.; Huskens, J. Cyclodextrin-based supramolecular nanoparticles stabilized by balancing attractive host-guest and repulsive electrostatic interactions. *Chem. Commun. (Cambridge, U. K.)* **2014**, *50* (55), 7280−7282.
(45) Xiong, F.; Ling, X.; Chen, X.; Chen, J.; Tan, J.; Cao, W.; Ge, L.; Ma, M.; Wu, J. Pursuing Specific Chemotherapy of Orthotopic Breast Cancer with Lung Metastasis from Docking Nanoparticles Driven by Bioinspired Exosomes. *Nano Lett.* **2019**, *19* (5), 3256−3266.
(46) Canton, I.; Battaglia, G. Endocytosis at the nanoscale. *Chem. Soc. Rev.* **2012**, *41* (7), 2718−2739.
(47) Canton, J.; Neculai, D.; Grinstein, S. Scavenger receptors in homeostasis and immunity. *Nat. Rev. Immunol.* **2013**, *13* (9), 621−634.
(48) Vance, J. E.; Karten, B. Niemann-Pick C disease and mobilization of lysosomal cholesterol by cyclodextrin. *J. Lipid Res.* **2014**, *55* (8), 1609−1621.
(49) Okada, Y.; Ueda, E.; Kondo, Y.; Ishitsuka, Y.; Irie, T.; Higashi, T.; Motoyama, K.; Arima, H.; Matuso, M.; Higaki, K.; Ohno, K.; Nishikawa, J.; Ichikawa, A. Role of 6-O-alpha-maltosyl-beta-cyclodextrin in lysosomal cholesterol deprivation in Npc1-deficient Chinese hamster ovary cells. *Carbohydr. Res.* **2018**, *455*, 54−61.
(50) Qian, H.; Zhao, X.; Cao, P.; Lei, J.; Yan, N.; Gong, X. Structure of the Human Lipid Exporter ABCA1. *Cell* **2017**, *169* (7), 1228.
(51) Okada, Y.; Ueyama, K.; Nishikawa, J.; Semma, M.; Ichikawa, A. Effect of 6-O-alpha-maltosyl-beta cyclodextrin and its cholesterol inclusion complex on cellular cholesterol levels and ABCA1 and ABCG1 expression in mouse mastocytoma P-815 cells. *Carbohydr. Res.* **2012**, *357*, 68−74.
(52) Bjorkhem, I.; Andersson, O.; Diczfalusy, U.; Sevastik, B.; Xiu, R. J.; Duan, C.; Lund, E. Atherosclerosis and sterol 27-hydroxylase: evidence for a role of this enzyme in elimination of cholesterol from human macrophages. *Proc. Natl. Acad. Sci. U. S. A.* **1994**, *91* (18), 8592−8596.

https://doi.org/10.1021/acs.nanolett.1c03664
Nano Lett. 2021, 21, 9736−9745

(53) Ouimet, M.; Barrett, T. J.; Fisher, E. A. HDL and Reverse Cholesterol Transport. *Circ. Res.* **2019**, *124* (10), 1505−1518.
(54) Pitha, J.; Gerloczy, A.; Olivi, A. Parenteral hydroxypropyl cyclodextrins: intravenous and intracerebral administration of lipophiles. *J. Pharm. Sci.* **1994**, *83* (6), 833−837.

https://doi.org/10.1021/acs.nanolett.1c03664
Nano Lett. 2021, 21, 9736−9745